Frequency modulation of laser radiation reflected from an expanding laser-produced plasma

R. Dragila, R. A. M. Maddever, and B. Luther-Davies
Laser Physics Centre, Institute of Advanced Studies, Research School of Physical Sciences, Australian National University, Canberra, Australian Capital Territory 2601, Australia
(Received 16 September 1986; revised manuscript received 18 May 1987)

$1\omega_0$ spectra from laser-produced plasmas have been observed at several angles to the backscattered direction with the use of very-large-F-number ($F=25$) collection optics. The spectra, produced by a single beam high-intensity ($I_0 < 10^{17}$ W/cm^2) Nd:glass laser incident on glass slab targets, are variously broadened, asymmetric, and red shifted with respect to the Doppler-shifted fundamental frequency, and display an irregular fine structure. These features are interpreted as due to the action of processes which modify the density profile and the expansion velocity of the critical surface, causing the phase of the outgoing light to vary nonlinearly in time. An analytic model is developed which shows that these features can be described primarily in terms of τ, the time scale for the phase modulation. The experimental results are compared with simulations using a one-dimensional computer code and reasonable agreement is obtained.

INTRODUCTION

The light emitted from a laser-produced plasma contains important information on details of the interaction between the incident heating beam and the plasma itself. In particular, the spectra near the laser frequency ($1\omega_0$) and its second harmonic ($2\omega_0$) are affected by processes occurring near the critical density surface. By analyzing such spectra it is, therefore, possible to obtain information on parameters such as the critical surface velocity, or to detect the presence of plasma waves (excited by either parametric processes or linear mode conversion), or the presence of ion acoustic waves in this important region. Many experimental studies have therefore been made of these spectra[1–8] (see Refs. 1–7 for a discussion on the backscattered $1\omega_0$ spectra and Ref. 8 for an extensive review of the second harmonic). In interpreting the results there are basically three physical processes that have been invoked.

Firstly, motion of the critical surface will Doppler shift the frequency of the light reflected from it (in the case of the fundamental frequency), or generated at it (in the case of the second harmonic). Since the critical surface velocity may vary in time, the Doppler effect can both shift and broaden the time-integrated emitted spectrum.

Secondly, the incoming laser radiation can be scattered off ion waves (Brillouin scattering) in the underdense region. As the incident high-frequency electromagnetic wave pumps the low-frequency ion acoustic wave during this process, the emergent scattered wave is either red shifted relative to the laser frequency if the plasma flow is subsonic, or blue shifted if the flow is supersonic. Since the spectrum of ion acoustic waves involved may itself be rather wide, this mechanism can result in the spectrum of the scattered light being broadened and red shifted (or blue shifted depending on the character of the plasma flow). Alternatively, a special case of Brillouin scattering can occur if ion waves with a well-defined frequency are generated in the critical region via some other independent process (e.g., the return current-driven ion acoustic instability). In that case the spectrum of the fundamental or second harmonic can become modulated in the manner discussed by Cairns[9] through the generation of multiple sidebands which will add a fine-structure component to the overall spectrum.

Thirdly, at the critical surface itself, the incoming laser radiation can couple to plasma waves either by linear mode conversion (resonance absorption) or via the parametric decay instability. In the former case the frequency of the plasma wave equals the laser frequency, while the parametric decay instability causes the excitation (or absorption) of an additional ion acoustic wave which frequency-shifts the plasma wave to the red (or blue) of the laser line. Beating between the incoming laser radiation and these plasma waves can result in the emission of radiation at frequencies close to the harmonic of the laser light. In the case where the parametric instability is involved a typically asymmetric, broad red-shifted second-harmonic spectrum results, while linear conversion produces a Doppler-shifted $2\omega_0$ spectrum which has a narrow spectral width approximately that of the incident laser radiation.

The fine interplay between all these mechanisms can lead to the spectra being very complex and difficult to interpret. However, by careful attention to the variations in the spectrum induced by changing parameters such as the laser light intensity, its polarization, and its angle of incidence at the target surface, it has been possible to isolate and characterize a variety of these processes. One feature which has so far received little attention, however, is the presence of modulations in the emitted spectrum. In fact, it has been only recently[10] that we, in this laboratory, have observed distinct modulation of the second-harmonic spectra similar to those predicted by Cairns.[9] The important feature of these previous experiments was the fact that second-harmonic emission was

collected by an array of optical fibers placed at different angles relative to the target surface and that each fiber collected radiation over a very narrow range of angles. This narrow collection angle ($F=25$) was vital in revealing the fine structure since it was evident that when the emission was averaged over a range of angles (such as has been the case when the spectra have been recorded by collecting the radiation using the focusing lens) the fine structure was smeared out and disappeared.

It was conjectured in his earlier work that the apparently regular fine structure might be due to the presence of ion acoustic waves generated by the flux of cold electrons propagating into the critical region to compensate for the ejection of hot electrons down the plasma density gradient by resonance absorption. Such a turbulence, if in the steady state, would have a Kadomtsev-Petviashvili spectrum,[11] $N(k)\propto k^{-4}$. This spectrum is highly peaked since it is abruptly cutoff at some wave number $k_{\min}$ defined by the longest wavelength ion wave that the plasma could support. We related $k_{\min}$ to the plasma-density gradient near critical, L: $k_{\min}\approx L^{-1}$, where $L=[n(dn/dx)^{-1}]_{n=n_c}$. This was equivalent to the spacing of ≈ 2 Å observed at that time.

In more recent work, using improved techniques, we attempted to better characterize the modulation frequency by applying Fourier analysis to the results and so determine its variation with parameters such as laser intensity and pulse duration. At the same time we extended our previous studies to record spectra at the laser frequency (ω_0) and observed that these, too, were modulated in a way similar to the second-harmonic spectra. To summarize the results of this more recent work, we have found that Fourier analysis failed to identify any specific modulation frequency characterizing our apparently highly modulated spectra. Furthermore, if any characterizing "modulation" frequency ($\Delta\mu$) could be discerned from the Fourier analysis, that frequency was too *low* to modulate the spectrum during the shortest duration pulses (20 psec) used in these studies (i.e., $\Delta\mu^{-1}\approx 20$ psec). For these two reasons, therefore, we found it necessary to discount our previous explanation involving modulation via externally generated ion waves and develop a new theory to explain our now better-characterized, larger quantity of data.

We will begin by discussing our experimental results, and firstly we will present a more detailed analysis of the $2\omega_0$ spectra than previously published,[10] which shows that the spectral modulations tend towards a chaotic nature and cannot be characterized by a single modulation frequency. We then present a larger body of data on the spectrum of the reflected laser light (near ω_0).

A wide range of target materials has been used in these experiments, including carbon fibers, 140-μm-thick glass slabs, and 0.5-mm-thick lead targets. The laser pulse duration was varied between a minimum of 20 psec to a maximum of 400 psec and the laser intensity between 1×10^{13} and $\approx 3\times 10^{17}$ W/cm^2 at wavelengths of 1.064 and 1.053 μm. The 20-psec duration pulses were generated using an active and/or passive mode-locked Nd:YAG oscillator (where YAG is yttrium aluminum garnet) which was later replaced with an all-active AMQ (actively mode-locked Q-switched) Nd:YLF oscillator[12] providing a minimum pulse duration of about 70 psec. The intensity on target was varied by moving the target in and out of the focal plane of the ($F=1$) aspheric doublet lens such that the focal-spot size ranged between 5 and 300 μm in diameter. The targets were generally oriented normal to the heating beam and were surrounded by five optical fibers arranged at angles of 0°, 35°, 50°, 65°, and 80° from the backscattered direction (Fig. 1). These fibers, and a sixth for the fiducial, transmitted light to the slit of a 1-m spectrograph where either the 1-μm spectra were recorded on Kodaz IZ plates, or the $2\omega_0$ spectra were recorded on Tri-X film. Despite the very high fluxes of $1\omega_0$ light being received at the film plane, it was found necessary to hypersensitize the plates prior to exposure. The procedure chosen was that described by Pope and Kirby[13] in which the plates were bathed with constant agitation in three consecutive baths: (1) 0.006% vol % solution of ammonium hydroxide in distilled water for 3 min, (2) 2 vol % of acetic acid in 90 vol % methyl alcohol for 1 min, and (3) 90 vol % methyl alcohol for 3 min. The plates were blown dry with the blower of a portable evaporative air conditioner at a temperature of about 22 °C. No safelight is available for such work so all was done in total darkness. Although the baths were kept in the region of 5 °C, in accordance with the recommendations of Pope and Kirby, using ordinary darkroom trays immersed in an ice and water bath, the air-conditioner temperature was a long way from the suggested 8 °C. However, in practice, our results were insensitive to this temperature. After exposure the plates were developed in Kodak D19 for 4 min.

In Figs. 2(a)–2(d) we present sample sets of $2\omega_0$ spectra obtained using laser pulse lengths of 20–400 psec incident of glass targets with the laser intensity being within the range $0.5-1.8\times 10^{15}$ W/cm^2 and the energy within 1–2 J. (Note that the signal level in fiber 1 was anomalously low for the 20-psec pulses, probably due to a break in the optical fiber.) We found that the spectra were insensitive to target material and have therefore only presented results recorded using glass targets. The

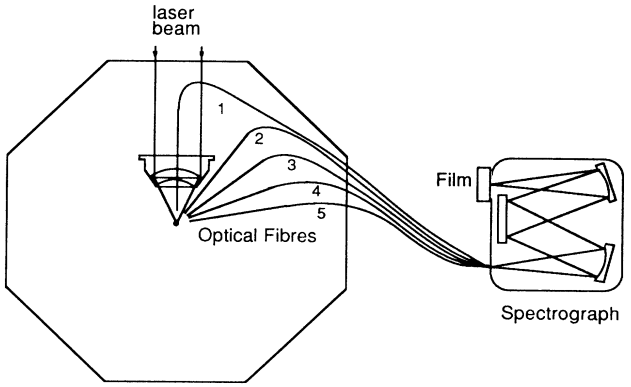

FIG. 1. Experimental arrangement for recording either $1\omega_0$ or $2\omega_0$ spectra (a sixth fiber, not shown, transmits the fiducial to the spectrograph).

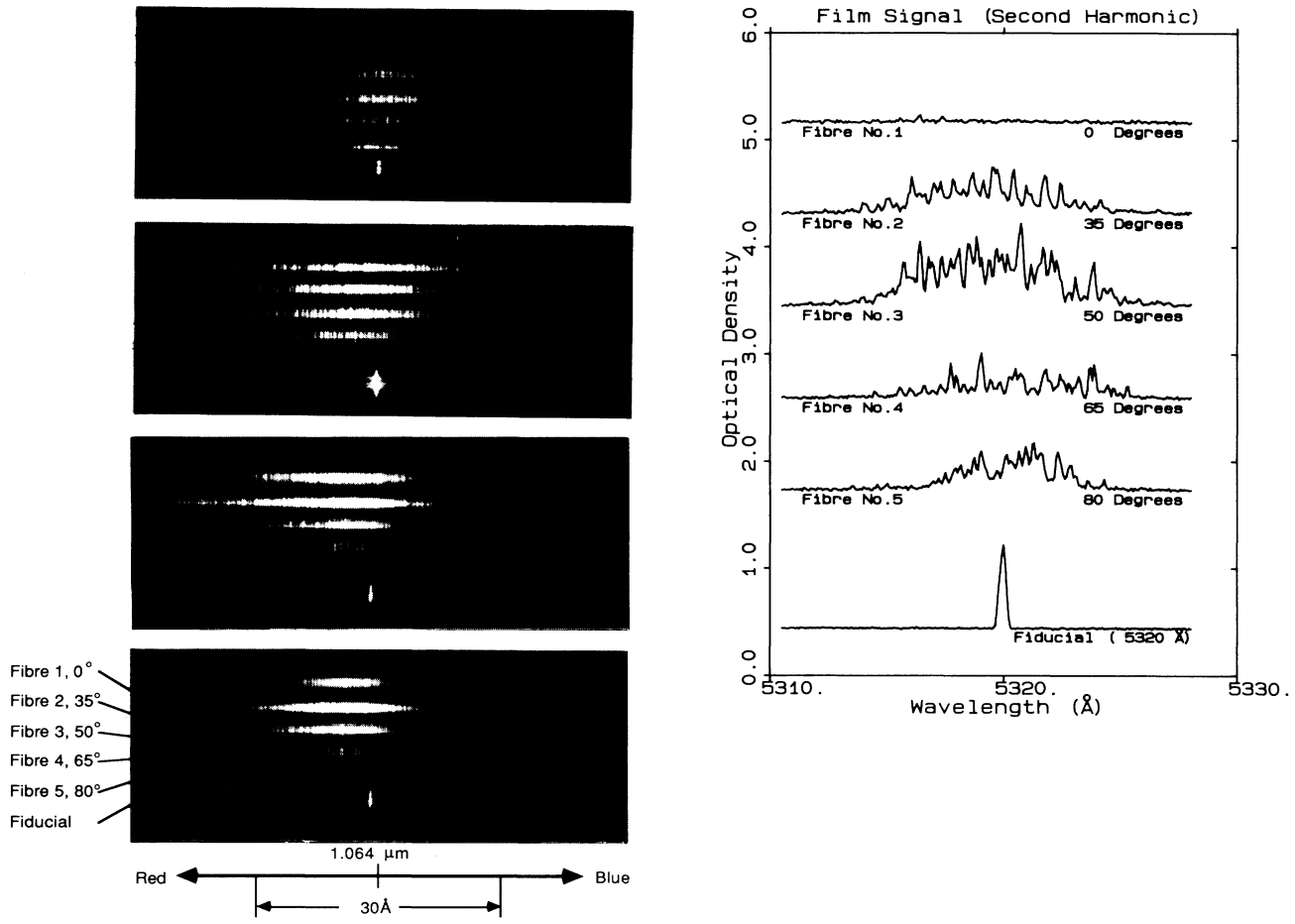

FIG. 2. Set of time-integrated $2\omega_0$ spectra obtained using a laser of wavelength 10 640 Å incident on planar glass targets with pulse lengths (a) 20 psec, (b) 100 psec, (c) 200 psec, and (d) 400 psec. The energy was within the range 1–2 J, the intensity $0.5-1.8\times10^{15}$ W/cm^2, and the experimental setup was that of Fig. 1. The five angles refer to the direction of view of the optical fibers relative to the backscatter direction. A sixth fiber indicates the $2\omega_0$ fiducial (5320 Å). (e) Microdensitometer traces of the 20-psec data in Fig. 2(a).

important thing to note in Fig. 2 is that the basic characteristics of the modulation did not vary significantly even though the laser pulse length was changed by over one order of magnitude. This is an important observation, since as the pulse duration is changed, parameters such as the plasma density scale length would be expected to vary and clearly such changes have very little effect on the spectra. The equivalent microdensitometer scans of the 20-psec data of Fig. 2(a) are shown in Fig. 2(e). As is evident, the spectra are highly modulated and at first sight give the impression that they can be characterized by an average modulation spacing of about 0.5 Å. However, such an impression is wrong, as is shown by the following quantitative analysis. The signal optical density was first converted via the film response curve to intensity. In order to isolate the modulations in the spectrum, the broad envelope, obtained by heavy smoothing, was divided into the original data within a suitable window. This resulted in a signal which weighted all modulations equally. A Hamming window was applied to the remaining signal and the power spectrum of the modulations then obtained from the Fourier transform in the usual way. These are shown in Fig. 3. If the modulations were regular, such an analysis would produce a single peak in the resulting power spectrum. Furthermore, the position of the peak would be expected to be the same for all viewing directions. Inspection of Fig. 3 shows that this is far from the case, with the power spectrum being characterized by a set of multiple peaks whose position and intensity varies randomly from shot to shot, and randomly between the different fibers for the same laser shot. This led us to the conclusion that, in spite of the apparent regular modulations one is tempted to identify from the raw data, in truth the $2\omega_0$ spectra are *randomly* modulated and no modulation frequency can be assigned. Clearly this conclusion runs counter to the idea that the modulations are caused by a monochromatic ion wave.

Additionally, if a region of dominance exists in Fig. 3 at all, it lies between 1 and 3 Å^{-1} which would correspond to a "modulation frequency" of between 1×10^{11} and 3×10^{10} Hz (and periods between 10 and 33 psec).

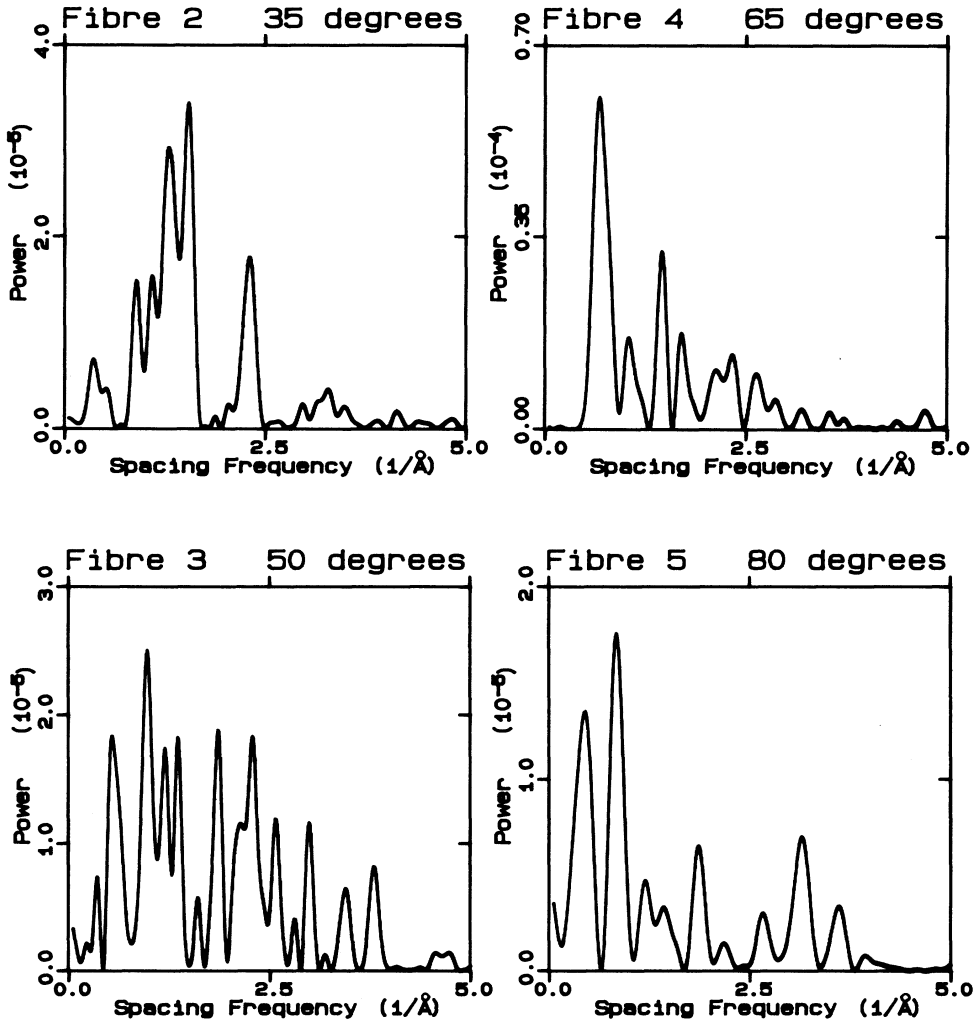

FIG. 3. "Film power spectra" obtained from the digitized signals in Fig. 2(e) by first dividing the data by their broad envelope, applying a Hamming window to the result, and Fourier transforming in the usual way.

Since the laser pulse duration was only one or two modulation periods long it is difficult to accept that any modulation of this kind could take place. These conclusions led us to study additional data, particularly on the spectrum of the $1\omega_0$ emissions, in an attempt to better characterize the modulations and to develop a new theory to describe their formation. The remaining part of the paper describes this work.

In what follows we concentrate on a description of the results of measurements of the backreflected $1\omega_0$ spectra. Qualitatively, these spectra display the same characteristic as those taken at $2\omega_0$ and, hence, we expect the mechanism leading to the specific spectral features in which we are interested—modulation and broadening—to be the same. It was found that the $1\omega_0$ spectra were more reproducible on a shot-to-shot basis and hence more suitable for a systematic study. We stress, however, that our comments are generally applicable to the $2\omega_0$ data as well. This is in itself quite important since obviously different physical processes are responsible for backreflection of the laser light and second harmonic generation, yet an explanation of the modulations must be equally applicable to both.

This later work was performed using the AMQ oscillator and the pulse duration was, therefore, in the range 70–400 psec. Once again the pulse duration did not affect the characteristics of the spectra in any significant fashion, with spectra recorded with 70- and 400-psec-duration pulses at about the same intensity being essentially indistinguishable.

A sample set of $1\omega_0$ spectra is shown in Fig. 4, recorded for laser intensities between 3×10^{13} and 5×10^{15} W/cm^2, using 100-psec-duration pulses and laser energies of approximately 2.5 J. Note that in this case the resolution was not as good as that used for the $2\omega_0$ spectrum shown in Fig. 2, and was limited by the 100-μm slit width on the monochromator to 1 Å. In general, the $1\omega_0$ spectra are characterized by the following features: (1) a broad, asymmetric, envelope peaking, usually on the blue side of the laser line which becomes broader with increasing laser intensity; (2) fine structure which tends to become considerably clearer as the incident

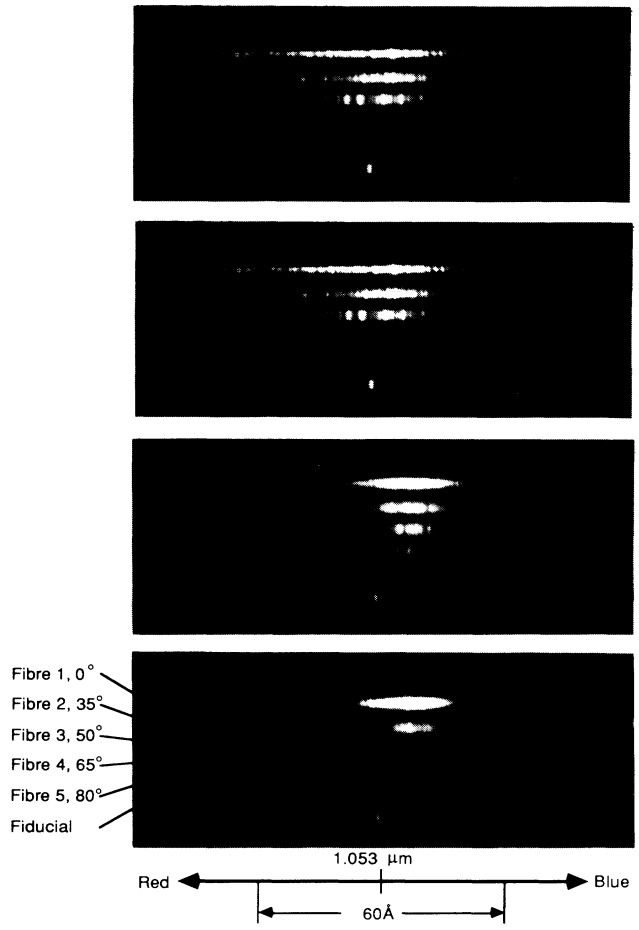

FIG. 4. Time-integrated $1\omega_0$ spectra produced by planar glass targets irradiated with a laser of wavelength 10 530 Å, pulse length 100 psec, energy 2.5 J, and incident intensities of (a) 5×10^{15} W/cm^2, (b) 1×10^{15} W/cm^2, (c) 3×10^{14} W/cm^2, and (d) 3×10^{13} W/cm^2.

pulse intensity increases above $I_0\approx5\times10^{14}$ W/cm^2 and which displays a poorly defined modulation spacing in the range of 1–3 Å; and (3) a blue shift which decreases with increasing laser intensity.

Notice the increased visibility of the modulation and the spectral broadening as the laser intensity is increased, and also the reduction in the blue shift. In the case of the lowest-intensity shot the blue shift is close to that expected from the Doppler effect alone for a plasma with an electron temperature of 500 eV ($\Delta\omega_D=2\mathbf{k}\cdot\mathbf{v}_c$ which implies $\Delta\lambda_D=11$ Å for a critical-surface velocity $\mathbf{v}_c=1.5\times10^7$ cm/s) and the modulations have all but disappeared. The blue shifts obtained from the directly backscattered spectra (fiber 1) are plotted as a function of intensity in Fig. 5. The position of the peak of the spectral envelope, which is plotted here, is rather difficult to determine, especially at high intensities—hence the larger scatter. Note that at the low-intensity end of the figure the curve tends towards an asymptotic shift of 10 Å. This result suggests that the mechanism responsible for broadening and modulating the spectrum

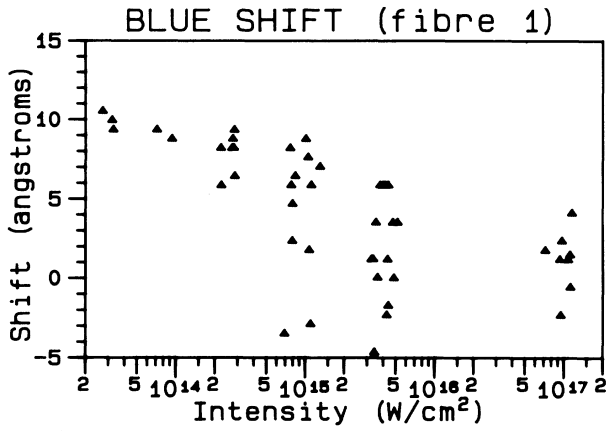

FIG. 5. The blue shift of the peak of the directly backscattered (fiber 1) $1\omega_0$ spectral envelope as a function of incident intensity.

basically shifts the radiation to the red of the normally blue Doppler-shifted emission.

We again applied Fourier analysis to search for a specific modulation frequency in these spectra using the method described above. In Fig. 6 the Fourier power spectra of the modulations are shown for the spectra in Fig. 4(b). Close examination of these data again fails to identify a single peak but rather shows a confusion of peaks which do not occur at the same position in the spectra obtained from the different fibers for a given laser shot and which, on a shot-to-shot basis, display no real consistency.

A study of the very large amount of ω_0 data similar to that presented above (about 100 sets of spectra) reinforced our conclusion that the spectral modulations are basically random and it was therefore necessary to develop a new explanation of this phenomenon. We have come to the conclusion that the modulations, the frequency shift, and the spectral broadening may all be generated by any process, including the hydrodynamic expansion of the plasma that induces a time-dependent nonlinear phase shift on the emergent electromagnetic (EM) wave. A simple linear phase shift in time leads to a Doppler shift as is well known. However, once the phase shift becomes nonlinear which can readily occur, for example, once the effect of the time-varying ponderomotive force on the plasma density profile (and hence its refractive index profile) is taken into account, the spectrum can become much more complex as will be demonstrated.

The influence of nonlinear phase modification has been discussed previously. It has been used successfully by Cheung *et al.*[14] to explain the spectral structure of small-scale trapped filaments of laser light in various liquids and also by Gorbunov[15] and Yamanaka *et al.*[16] in their analyses of reflected light originating either from self-focusing in a laser-produced plasma, or from the modulation instability due to resonance absorption in the region of the cutoff density. However, as far as we know, this is the first time that it has been demonstrated that a much simpler process, involving the plasma hy-

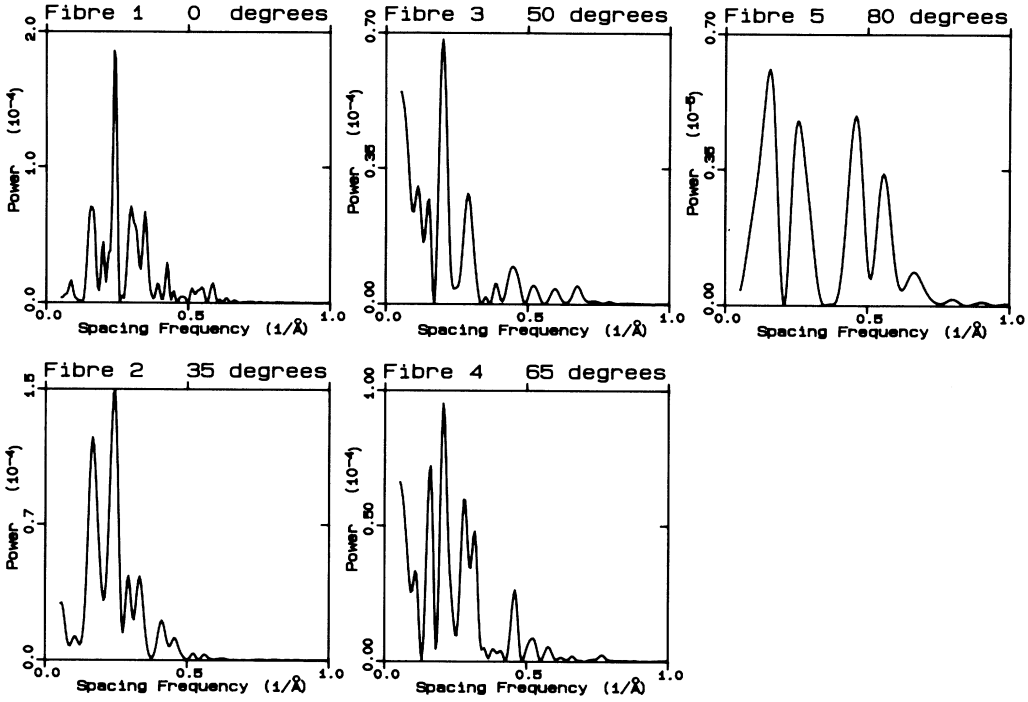

FIG. 6. "Film power spectra" obtained from the data of Fig. 4(b).

drodynamics, has been used to explain the various features of the backscattered spectra, and this has important ramifications for the spectra of other harmonics and low-intensity probe pulses passing through, or being reflected by, the plasma.

THEORY

To introduce the effect of the nonlinear phase shift on the emitted spectrum we will concentrate on the simplest case when the hydrodynamic expansion of the plasma is affected by the time-dependent ponderomotive force and this leads to nonlinear phase variations in the emergent EM waves.

We will first consider a simplified model of an inhomogeneous stratified plasma occupying a half space $x > x_0$. We assume that there is a plane $x = x_E > x_0$ within the plasma representing a source of emission of a coherent plane wave with frequency ω_0. The wave vector of the emitted wave is assumed to have a nonzero component along the plasma density gradient $k_x < 0$. Finally, we assume that the optical thickness of the plasma slab between $x = x_0$ and x_E varies slowly in time as does the amplitude of the wave E_0 which we will, therefore, initially consider to be a constant. The temporal density variations result in temporal variations of the phase $\phi = \phi(t)$ of the emitted wave, $E(t)$,

$$E(t) = E_0 \cos[\omega_0 t - \phi(t)] , \tag{1}$$

where $E_0 = \text{const}$ and $|d\phi/dt| \ll \omega_0$. Then the spectral intensity of the emitted radiation becomes

$$I(\omega) = \tfrac{1}{4} I_0 [\, |J(\omega,\phi)|^2 + J(\omega,\phi)J(-\omega,\phi) + |J(-\omega,\phi)|^2 + J^*(\omega,\phi)J^*(-\omega,\phi)] , \tag{2}$$

where

$$J(\omega,\phi) = \int_{-\infty}^{\infty} \exp[i(\omega-\omega_0)t + i\phi(t)]dt \tag{3}$$

and

$$I_0 = \frac{c}{4\pi} E_0^2 .$$

From the definition (3), $J(\omega,\phi)$ has a maximum for $|\Delta\omega| \ll \omega_0$, where $\omega - \omega_0 = \Delta\omega \equiv -d\phi/dt$. Therefore, $|J(-\omega,\phi)| \ll |J(\omega,\phi)|$ and one can approximate

$$I(\omega) = \tfrac{1}{4} I_0 |J(\omega,\phi)|^2 . \tag{4}$$

To evaluate the integral $J(\omega,\phi)$ we use the method of stationary phase which makes the approximation that the average value of the integrand is only nonzero in the region where $-d\phi/dt \approx \omega - \omega_0$. However, before we proceed, we need to specify the shape of $\phi(t)$, at least qualitatively.

Firstly, we expect deviations of $\phi(t)$ from a basically linear shape (which would be due to motion of the critical surface at a constant velocity during the laser pulse) to be caused by the ponderomotive force. Its effects include (a) creation of a steep density profile in the vicinity of the critical surface with its lower-shelf density dropping as the pulse intensity increases, and rising after the peak of the pulse, and (b) deceleration of the critical surface by increasing ponderomotive pressure and subse-

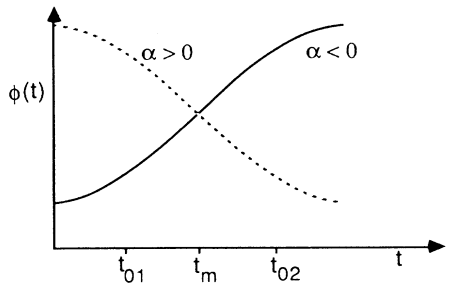

FIG. 7 A simple case of the phase function $\phi(t)$ as defined by Eq. (7). $t=t_m$ is that instant of time where $|d\phi/dt|$ is a maximum while t_{01} and t_{02} are two points of the stationary phase having the same value of $|d\phi/dt|$.

quent acceleration after the peak of the pulse. Therefore, generally, the increase and decrease of the ponderomotive force results in phase changes with respect to the unperturbed behavior which we qualitatively show in Fig. 7 [for the simplest case in $\phi(t)$]. The most important feature is the presence of the point of inflection at some $t=t_m$. Mirror reflection at $t=t_m$ or rotation around the point $[t_m,\phi(t_m)]$ bring no new features into this effect. Thus $t=t_m$ is that instant of time where $|d\phi/dt|$ is a maximum (in general, a maximum deviation with respect to $|d\phi/dt|_{t=0}$). Within the limits $\omega\in\langle\omega',\omega''\rangle$ defined by

$$\omega'=\omega_0,\quad \omega''=\omega_0+\Delta\omega_{\max}>0$$

and

$$\omega'=\omega_0+\Delta\omega_{\max},\quad \omega''=\omega_0 \text{ for } \Delta\omega_{\max}<0\ ,$$

where

$$\Delta\omega_{\max}\equiv\left[\frac{-d\phi}{dt}\right]_{t=t_m},$$

there are always two points t_{01} and t_{02} $(t_{01}<t_{02})$ of the stationary phase having the same value of $|d\phi/dt|$ for any given ω. Note that t_{01} equals t_{02} for $\omega=\omega_0+\Delta\omega_{\max}$. $J(\omega,\phi)$ can now be approximated as follows:

$$J(\omega,\phi)=\left[\frac{\pi}{2}\right]^{1/2}\sum_{j=1}^{2}\exp\{i[\tfrac{1}{4}\pi+\Delta\omega\, t_{0j}+\phi(t_{0j})]\}\times\left[\frac{d^2\phi}{dt^2}\right]^{-1/2}_{t=t_{0j}},\tag{5}$$

and the spectral intensity of emitted radiation becomes, according to (4),

$$I(\omega)=\frac{\pi}{8}I_0(|A_1|^2+|A_2|^2+2\,\mathrm{Re}\,A_1A_2^*\exp\{i[\Delta\omega(t_{01}-t_{02})+\phi(t_{01})-\phi(t_{02})]\}),\tag{6}$$

where

$$A_j=\left[\frac{d^2\phi}{dt^2}\right]^{-1/2}_{t=t_{0j}},\quad j=1,2\ .$$

To demonstrate the role of temporal modulation of the plasma optical thickness we will assume a specific form of $\phi=\phi(t)$ as follows:

$$\phi(t)=\alpha[1+\cos(\pi t/\tau)]+\phi(\tau)\tag{7}$$

for $t\in\langle 0,\tau\rangle$, where τ is a characteristic time scale of the phase (or plasma) temporal variations. Then

$$\Delta\omega_{\max}=\alpha\pi/\tau\tag{8}$$

and $t_m=\tau/2$. Further, for a fixed value of $\Delta\omega$ there are two points of stationary phase,

$$t_{01}=\frac{\tau}{\pi}\arcsin\left[\frac{\Delta\omega}{\Delta\omega_{\max}}\right],\qquad t_{02}=\tau-t_{01}\ .\tag{9}$$

The coefficients $A_{1,2}$ then become

$$A_{1,2}=\left[\frac{\alpha}{\pm(\Delta\omega_{\max})^2\cos[\arcsin(\Delta\omega/\Delta\omega_{\max})]}\right]^{1/2}\tag{10}$$

(where A_1 takes the plus sign in the denominator and A_2 takes the minus sign) and therefore

$$I(\omega)=\frac{I_0\pi\alpha}{4(\Delta\omega_{\max})^2\cos[\arcsin(\Delta\omega/\Delta\omega_{\max})]}\times\left[1+\sin\left\{\frac{2\,\Delta\omega\,\tau}{\pi}\left[\arcsin\left[\frac{\Delta\omega}{\Delta\omega_{\max}}\right]-\frac{\pi}{2}\right]+2\frac{\Delta\omega_{\max}\tau}{\pi}\cos\left[\arcsin\left[\frac{\Delta\omega}{\Delta\omega_{\max}}\right]\right]\right\}\right].\tag{11}$$

The argument of the sin function in (11) falls within the interval $\langle 0,2\alpha\rangle$ and therefore $I(\omega)$ has an oscillatory character for $\omega'\le\omega\le\omega''$ and $\alpha\ge 1$. The number of peaks in such a modulated spectrum is then

$$N=|\alpha/\pi|\ ,$$

and consequently the average separation of the peaks, in rad/sec, is

$$\delta\omega=|\Delta\omega_{\max}|/N=\pi^2/\tau\ .\tag{12}$$

This result is quite general and is independent of details in the form of $\phi(t)$ as assumed by (7). For a fixed characteristic time scale τ of the phase temporal variations, the number of the peaks in the modulated spectrum is [see (6)]

$$N=\frac{\left|\left.\frac{d\phi}{dt}\right|_{t=0}\tau+\phi(0)-\phi(\tau)\right|}{2\pi}\ .$$

The increasing deviation of

$$\left.\frac{d\phi}{dt}\right|_{t=t_m} \text{ from } \left.\frac{d\phi}{dt}\right|_{t=0}$$

results in increasing width of the spectrum $\Delta\omega_{\max}$ and a proportional increase in number of peaks with the separation between the peaks remaining constant. This admittedly simplified example is useful because it illustrates the basic physical processes determining the spectrum. As is evident, the modulations are the result of the limited duration of the phase event which, on Fourier transformation, results in the generation of spectral modulations whose spacing is inversely proportional to that duration. The relative intensities of the modulations are affected by the fact that the modulations are multiplied in Fourier space by an envelope function derived from the shape of the phase curve. In practice, of course, the phase curve will not be a simple cosine function and its exact form must be calculated using some sort of computer model.

When the plasma slab together with the emitting plane, $x=x_E$, is in motion $x_E=x_E(t=0)-vt$ ($v>0$ is assumed constant) and perturbation of v and of the plasma optical thickness occurs within some time interval τ, the temporal variation of the phase ϕ of the emitting wave is qualitatively like that shown in Fig. 8. All of the previous analysis remains the same with the replacement

$$\omega_0\rightarrow\omega_0+\Delta\omega_D=\omega_0+(-d\phi/dt)_{t=0}\ ,$$

$$\Delta\omega\rightarrow -d\phi/dt-\Delta\omega_D\ ,$$

and

$$\Delta\omega_{\max}=(-d\phi/dt)_{t=t_m}-\Delta\omega_D\ ,$$

where $\Delta\omega_D$ represents the Doppler shift. The spectrum of the emitted radiation then falls within the range

$$\omega_0+\Delta\omega_D-|\Delta\omega_{\max}|<\omega<\omega_0+\Delta\omega_D \tag{13}$$

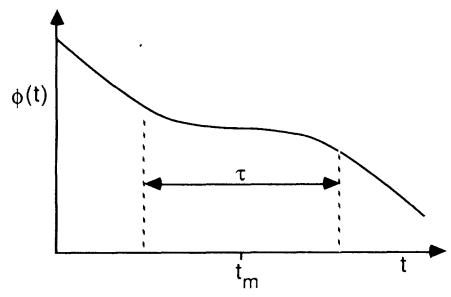

FIG. 8. A more realistic form of $\phi(t)$ which includes motion of the plasma slab and the emitting plane. τ is the time scale of the phase variation.

and is red shifted with respect to the Doppler-shifted line. Obviously, for a plasma slab moving in the opposite direction ($v<0$), $\omega_0+\Delta\omega_D<\omega<\omega_0+\Delta\omega_D+\Delta\omega_{\max}$, and the emission is red shifted with respect to the (red) Doppler-shifted line.

So far we have ignored the effect of amplitude variations of the wave on the emitted spectrum. Their effect is to convolve the spectrum resulting from the phase variations with an additional function representing the Fourier transform of the temporally varying amplitude. For $E_0=$const, this is of course a δ function and the spectrum is of the form described above. When $E_0=E_0(t)$, however, the convolving function may itself be complex and multiply peaked and in the situation where the characteristic time scale of these intensity variations are comparable with those of the phase variations the complexity of the spectral structure can increase considerably. It is worth noting that it is only the combination of the nonlinear phase shift where the instantaneously emitted frequency varies in time together with finite duration of the phase and/or amplitude event that can generate a broad modulated time-integrated spectrum of the form observed experimentally. Amplitude modulation of a broad spectrum with all frequencies emitted simultaneously will not lead to spectral modulations.

NUMERICAL CALCULATIONS

To obtain a more realistic feel for $\phi(t)$ and also to account for the variation in the velocity of the critical surface we have used a computer code which simulates conditions in the plasma. The Lagrangian code, which is described elsewhere,[17] is one dimensional, one fluid, two temperature, and includes real and artificial viscosities, electron heat conductivity and the ponderomotive force term. The numerical scheme is fully implicit and conservative. Maxwell's equations are solved for an Eulerian mesh which is redefined in each time step so that the mesh size is always fine enough ($\approx\lambda_0/20-\lambda_0/10$) within the region where WKB (geometrical optics) does not apply. To save computational time we also modify the Lagrangian mesh at each time step, refining the mesh within the vicinity of the critical region where profile modification and plasma density gradient steeping occurs. This transformation from one Lagrangian mesh to another is done in such a way that the mass, momentum, and internal energy are conserved.

Figure 9(a) shows the computer-generated time evolution of the density profile for a 100-psec Gaussian laser pulse of intensity $I_0=1\times10^{15}$ W/cm^2 incident on a glass target. Successive curves on the graph represent density profile "snapshots" taken every 20 psec. Note particularly the varying critical surface velocity and the density profile modification due to the action of the ponderomotive force. The phase function $\phi(t)$ generated by the code is shown in Fig. 9(b) and the corresponding frequency spectrum (with origin set to the true fundamental; $f>0$ represents a blue shift) which has been determined from the Fourier transform of the electric field, $E(t)\propto\sqrt{I(t)}e^{i[\phi(t)]}$, of the reflected wave is plotted in

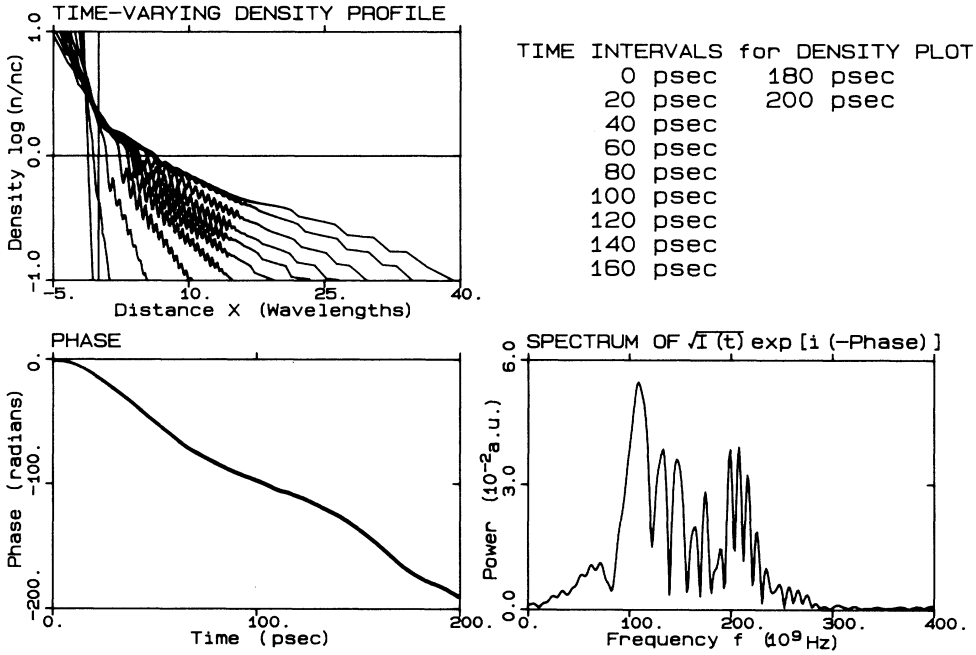

FIG. 9. (a) The computer-generated time evolution of the density profile for a 100-psec Gaussian laser pulse of intensity $I_0 = 1 \times 10^{15}$ W/cm^2 incident on a glass target. Successive curves on the graph represent density profile "snapshots" taken every 20 psec. (b) The phase function $\phi(t)$ generated by the code. (c) The corresponding frequency spectrum (with origin set to the true fundamental; $f > 0$ represents a blue shift) which has been determined from the Fourier transform of the electric field, $E(t) \propto \sqrt{I}(t) e^{i[\phi(t)]}$, of the reflected $1\omega_0$ wave. Here $I(t)$ represents the temporal envelope of the intensity of the reflected $1\omega_0$ wave, which incorporates the coefficient of reflectivity into the Gaussian variation of the laser pulse.

Fig. 9(c). Here $I(t)$ represents the temporal envelope of the intensity of the reflected $1\omega_0$ wave, which incorporates the coefficient of reflectivity into the Gaussian variation of the laser pulse. Obviously, the dominant frequencies in the power spectra are those defined by $f \sim -d\phi/dt$ at the center of the pulse.

In order to compare the calculated data with those of the experiment it is necessary to simulate the effect of the slit used when collecting the experimental data. Thus, we when we took the 1×10^{15} W/cm^2 spectrum of Fig. 9, convoluted it with a 100-μm slit, and then processed it in the same way as we did the experimental data (see Introduction), we obtained the numerical "film power spectrum" shown in Fig. 10.

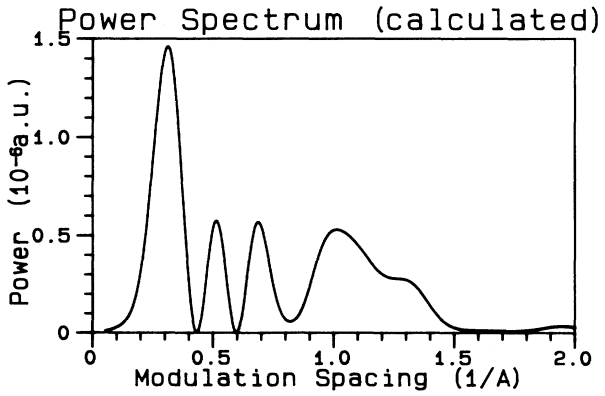

FIG. 10. Numerically simulated "film power spectrum" derived by convolving a 100-μm slit with the computer-generated spectrum in Fig. 9(c) and then processing the result in order to isolate the modulations just as was done for the experimental microdensitometer traces (cf. Figs. 3 and 6).

To get some information on how sensitive the spectrum is to the laser intensity we have run the code for several intensities. We show the corresponding plots for $I_0 = 1 \times 10^{14}$ W/cm^2 in Fig. 11. As expected, the ponderomotive force effects are weaker and the spectrum narrower, consistent with the experimental observation.

Our choice of relatively moderate intensities for comparison of calculated and experimental data is dictated mainly by two reasons. Firstly, the plasma is more or less classical in this region since there are not too many hot electrons and a relatively small portion of laser energy is involved in nonlinear processes. Secondly, the plasma flow conditions are more one dimensional here, becoming more and more three dimensional as the laser intensity is increased, due to the changing focal-spot size. Note that the strong modulations observed in the underdense region in the simulation are driven by the ponderomotive force associated with the standing wave generated by the interference of the incident and reflected wave—not by processes such as stimulated Brillouin scattering (SBS) which are not treated in the code.

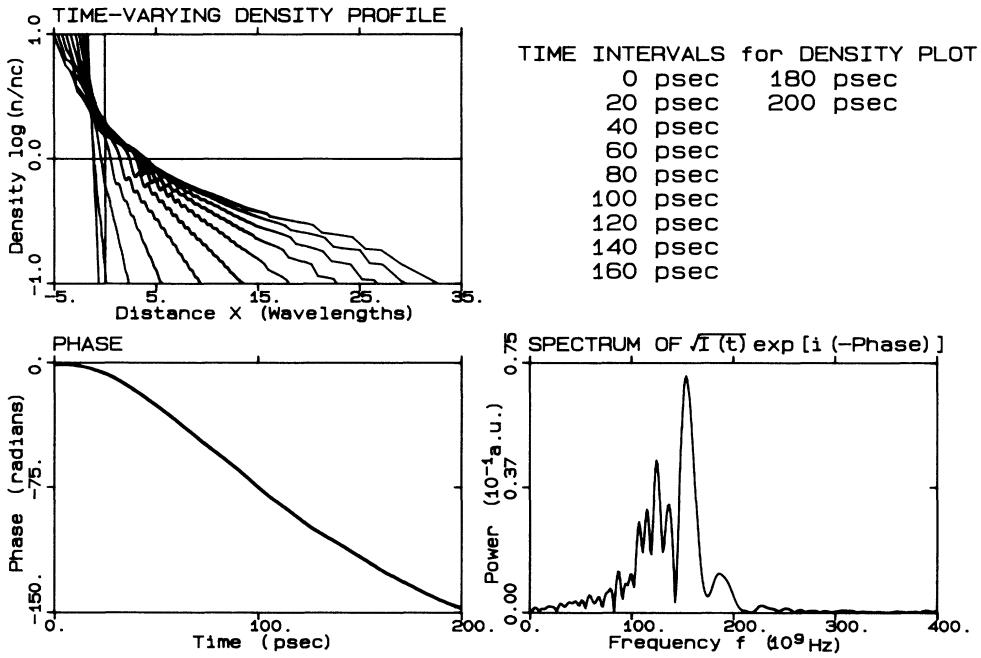

FIG. 11. The computer-generated result for a 100-psec Gaussian laser pulse of intensity $I_0 = 1 \times 10^{14}$ W/cm^2 incident on a glass target (see Fig. 9): (a) the time evolution of the density profile, (b) the phase function $\phi(t)$, and (c) the frequency spectrum.

DISCUSSION

The numerically obtained $1\omega_0$ power spectra, which are affected only by the phase variations induced by the hydrodynamics effect of the ponderomotive force, appear to agree at least qualitatively with experiment. For an intensity of 1×10^{15} W/cm^2 the modulation frequency of the calculated spectrum [Fig. 9(c)] lies in the range $\delta t \sim (1-5) \times 10^{10}$ Hz, which is equivalent to a spacing of 0.4–2.0 Å, while the corresponding experimental spectrum has a modulation spacing of approximately 2 Å. However, after convolution with a slit function of the same width of 100 μm as that used in the experiment, the high-frequency modulations in the numerical spectrum are smeared out, and the film power spectra (Figs. 6 and 10) then compare favorably.

Neither in the experiment nor in the numerical simulations does the spacing vary significantly with intensity and, furthermore, in both cases as the intensity increases the peak of the signal envelope shifts to the red, and the spectrum broadens. That this should be so, theoretically, is clear from Eq. (6) and the discussion following Eq. (12). Higher intensities produce a greater ponderomotive pressure and hence a larger phase modification, which, in turn, results in a greater value of $\Delta\omega_{\max}$ and a broader spectrum.

The main difference between experiment and theory lies in the detailed shape of the spectra. Those calculated are more asymmetric, usually peaking on the red end and decaying to the blue, while in the experiment the spectra are less asymmetric and display a peak towards the blue side. Such differences are not surprising since there are obvious limitations in the accuracy of the code (for example SBS is not treated, neither are two- and three-dimensional effects). Since the spectral details are extremely sensitive to even a slight modification of the phase function $\phi(t)$, it is clear that we should not expect to obtain exact agreement. To demonstrate this we have generated an artificial phase function [see Fig. 12(a)] which is, in fact, very close to those already calculated.

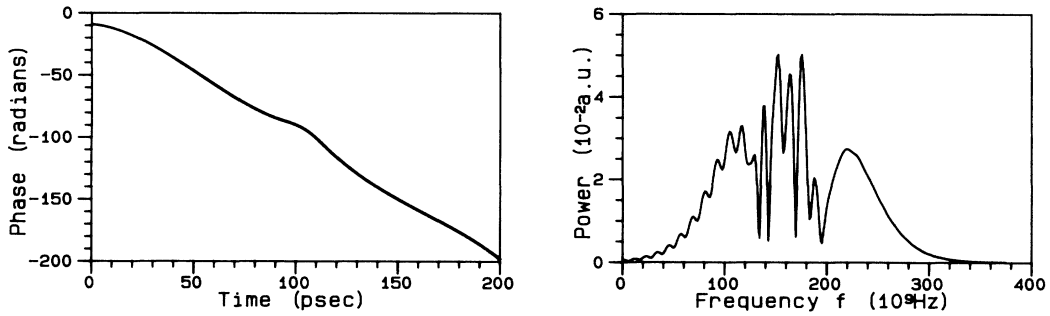

FIG. 12. (a) Hypothetical form of the phase function $\phi(t)$ which displays only slight flattening in the center of the pulse. (b) The corresponding power spectrum of $\sqrt{I}(t)e^{i[\phi(t)]}$ illustrating the sensitivity of the spectrum to the details of $\phi(t)$.

The perturbation introduced, in the form of only a slight flattening, results in the spectrum shown in Fig. 12(b). Since the blue spectral shift is proportional to $-d\phi/dt$ and the power in that contribution is proportional to $\sqrt{I(t)}$, at any instant, it is clear that, on the average, over the full length of the pulse, much more power now lies in the higher frequences than before, with the result that the envelope is considerably close to that which is observed in the experiment. Therefore, any temporal density variation on a laser-pulse time scale that is superimposed on a purely one-dimensional profile modification (as calculated by the code) results in broadening of the spectrum and modifies the shape of its envelope. Also, any temporal variation of the coefficient of reflectivity $|R|^2$ can affect the spectrum [this in effect changes the form of $I(t)$ which as discussed earlier, results in the spectrum being convolved with an additional multiply peaked function]. For example, if the laser light intensity close to the peak of the pulse exceeds the threshold of some anomalous absorption mechanism (e.g., ion acoustic turbulence or the parametric instability), there is a corresponding drop in $|R|^2$ and, consequently, an enhancement of the wings of the spectrum relative to the peak (effectively broadening the spectrum). This is demonstrated in Fig. 13(a) where we show the theoretical spectrum, calculated by the computer code, for the intensity $I_0 = 1 \times 10^{14}$ W/cm^2. The input parameters were identical to those which produced Fig. 11, except that in this case the parametric decay instability was allowed to operate by the incorporation of an effective collision frequency. Figure 13(b) gives a comparison of $|R|^2$ for the two cases.

One of the most important repercussions of the above analysis is that backscattered spectra whose red shift and fine structure have been attributed, in some previous papers, to Brillouin scattering may have to be reexamined. It has been shown here that almost identical features may also be produced purely by the ponderomotive-force-induced modification of both the density profile and the motion of the critical surface, provided $I_0\lambda^2$ is sufficiently large. The major way by which these two processes might be distinguished concerns directionality. Phase modification will occur to some extent no matter what direction the output ray emerges. In fact, for a one-dimensional expansion, the red shift is expected to *increase* with γ, the observation angle, and the blue Doppler shift will *decrease* by the factor $\cos\gamma$. The net result is that spectra taken at successively greater angles γ would shift further and further to the red. If the expansion is not one dimensional this effect is much reduced, and may not even be noticeable at all if the expansion is spherical. On the other hand, Brillouin scattering, because of its inherent directionality, would cause the red-shifted component to disappear as the observation angle moves away from the backscattered direction, as has been reported, for example, by Garban *et al.*[6] Additionally, the spectrum produced by SBS is in general characterized by the simultaneous emission of a broad band of frequencies. In that case we would not expect to be able to see modulations induced by phase variations in the emitted wave (or temporal modulation of the emission) as is the case here.

The obvious question regarding these results is: What form does the time-resolved spectrum take? According to the analysis presented here, the instantaneous emitted frequency should vary smoothly in time as has indeed been observed in experiments from Tarvin *et al.*[18] However, a very large body of information exists in the literature to suggest that in fact the intensity of both the $1\omega_0$ and $2\omega_c$ emissions, as well as other harmonics, are modulated in time with bursts only a few tens of picoseconds in duration.[7,19–23] This behavior is still consistent with our model since we only require the wave to undergo a nonlinear phase change induced by ponderomotive effects during these short pulses to generate the spectral modulations we observe. In fact, we have collected a very large amount of time resolved data, recording the intensity of both the ω_0 and $2\omega_0$ emissions, their spatial distribution, and their spectral characteristics. Our results show that both emissions do pulsate in accordance with previous data, with the frequency spectrum being broad and red shifted during those pulses. The uncertainty principle prevents a determination of whether the emission is frequency modulated during these bursts. However, we argue that to obtain the spec-

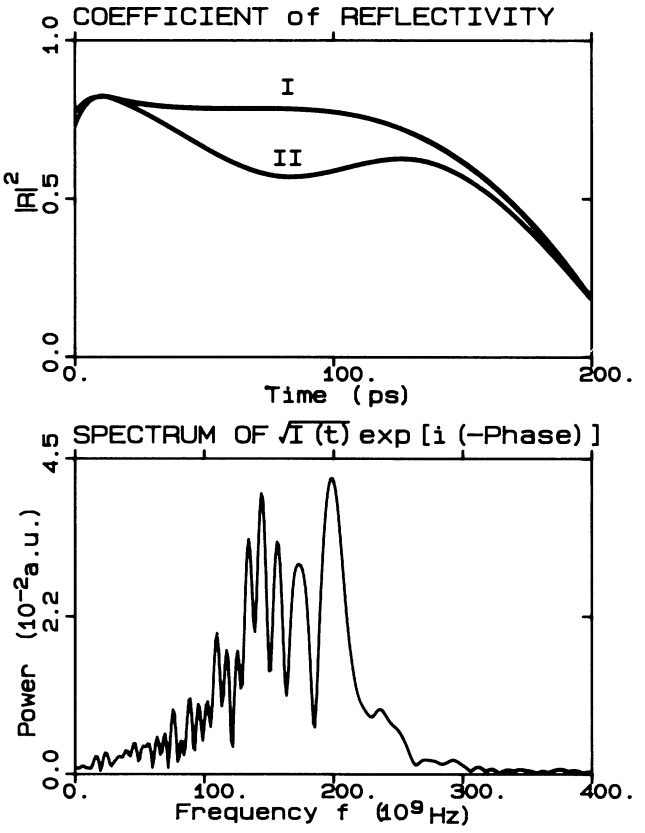

FIG. 13. (a) The computer-generated frequency spectrum of a 100-psec Gaussian laser pulse of intensity $I_0 = 1 \times 10^{14}$ W/cm^2 incident on a glass target—but now with the parametric density instability operating [cf. Fig. 11(c)]. (b) The intensity coefficient of reflectivity $|R|^2$ for the case of I without, and II with, parametric instabilities operating.

tral modulations in the time-integrated spectra, this *must* occur since simultaneous emission of a broad band of frequencies cannot result in such modulations. The presence of essentially random modulations in the time-integrated spectrum are, therefore, an important indication of the operation of this mechanism. We regard a full presentation of the time-resolved data and its interpretation as beyond the scope of this paper, but overall the time-resolved results indicate the operation of some (at present ill-understood) mechanism, which leads to the pulsations of the emission and determines the duration of the nonlinear phase event τ which in the theory section we had admittedly left somewhat ill defined.

CONCLUSION

We have successfully explained a number of features characterizing the emission spectra of the fundamental frequency of the heating beam of a laser-produced plasma by using a hydrodynamic model of profile modification by the ponderomotive force. The interpretation of the numerical results and comparison with experiment lead to the following observations: (1) the $1\omega_0$ spectrum is modulated with an approximate spacing corresponding to $\delta\omega \sim \pi^2/\tau$, where τ is the time scale of the nonlinear phase event induced by the plasma expansion, (2) the spectrum is red shifted with respect to the Doppler-shifted fundamental frequency, and (3) nonlinear variations of the phase function $\phi(t)$ are due to the both profile modification and variations in the velocity of the critical surface. However, we note that the simulated spectra display an envelope shape which differs in detail from experiment.

A consequence of the theory of phase modification by profile steepening is that all light which is reflected from the plasma, or originates sufficiently far inside the plasma, could display a fine structure of the kind discussed above. Since the modulation frequency depends only on the hydrodynamic time scale τ of the density profile then it should not differ significantly from harmonic to harmonic. The wavelength spacing will, of course, differ with the inverse square of the number of the harmonic n, i.e., $\Delta\lambda_n = (1/n^2)\Delta\lambda_1$.

[1]L. M. Goldman, J. Soures, and M. J. Lubin, Phys. Rev. Lett. **31**, 1184 (1973); J. Soures, L. M. Goldman, and M. J. Lubin, Nucl. Fusion **13**, 829 (1973).

[2]K. Eidmann and R. Sigel, in *Laser Interactions and Related Plasma Phenomena,* edited by H. Schwarz and H. Hora (Plenum, New York, 1974), Vol. 3B, pp. 667–690.

[3]B. H. Ripin, J. M. McMahon, E. A. McLean, W. M. Manheimer, and J. A. Stamper, Phys Rev. Lett. **33**, 634 (1974).

[4]K. B. Mitchell, T. F. Stratton, and P. B. Weiss, Appl. Phys. Lett. **27**, 11 (1975).

[5]E. Jannitti, A. M. Malvezzi, and G. Tondello, J. Appl. Phys. **46**, 3096 (1975).

[6]C. Garban, E. Fabre, C. Stenz, C. Popivcs, J. Virmont, and F. Amiranoff, J. Phys. Lett. (Paris) **39**, 165 (1978).

[7]D. R. Gray, J. Murdoch, S. M. L. Sim, A. J. Cole, R. G. Evans, and W. T. Toner, Plasma Phys. **22**, 967 (1980).

[8]N. G. Basov, V. Yu. Bychenkov, O. N. Krokhin, M. V. Osipov, A. A. Rupasov, V. P. Silin, G. V. Skilzkov, A. N. Starodub, V. T. Tikhonchuk, and A. S. Shikanov, Kvant. Elektron. (Moscow) **6**, 1829 (1979) [Sov. J. Quantum Electron. **9**, 1081 (1979)].

[9]R. A. Cairns, J. Plasma Phys. **22**, 149 (1979).

[10]M. D. J. Burgess, R. Dragila, and B. Luther-Davies, Opt. Commun. **50**, 236 (1984).

[11]V. Yu. Bychenkov and V. P. Silin, Zh. Eksp. Teor. Fiz. **82**, 1886 (1982) [Sov. Phys.—JETP **55**, 1086 (1982)].

[12]B. Luther-Davies, Opt. Commun. **57**, 345 (1986).

[13]T. P. Pope and T. B. Kirby, J. Opt. Soc. Am. **57**, 951 (1967).

[14]A. C. Cheung, D. M. Rank, R. Y. Chiao, and C. H. Townes, Phys. Rev. Lett. **22**, 786 (1968).

[15]L. M. Gorbunov, Zh. Eksp. Teor. Fiz. **84**, 1615 (1983) [Sov. Phys.—JETP **57**, 941 (1983)].

[16]C. Yamanaka, T. Yamakanka, J. Mizui, and N. Yamaguchi, Phys. Rev. A **11**, 2138 (1975).

[17]R. Draglia and J. Krepelka, J. Phys. (Paris) **39**, 617 (1978).

[18]J. A. Tarvin and R. J. Schroeder, Phys. Rev. Lett. **47**, 341 (1981).

[19]P. D. Carter, S. M. L. Sim, and T. P. Hughes, Opt. Commun. **27**, 423 (1978).

[20]P. A. Jaanimagi, G. D. Enright, and M. C. Richardson, IEEE Trans. Plasma Sci. **PS-7**, 166 (1979).

[21]P. D. Carter, S. M. L. Sim, H. C. Barr and R. G. Evans, Phys. Rev. Lett. **44**, 1407 (1980).

[22]Z. Liu, O. Willi, R. G. Evans, and J. Szechi, Rutherford Laboratory Report No. RL-82-106, 1982 (unpublished).

[23]Z. Liu, W. Tan, M. Gu, G. Mei, C. Pan, W. Yu, and X. Deng, Laser and Part. Beams **4**, 223 (1986).

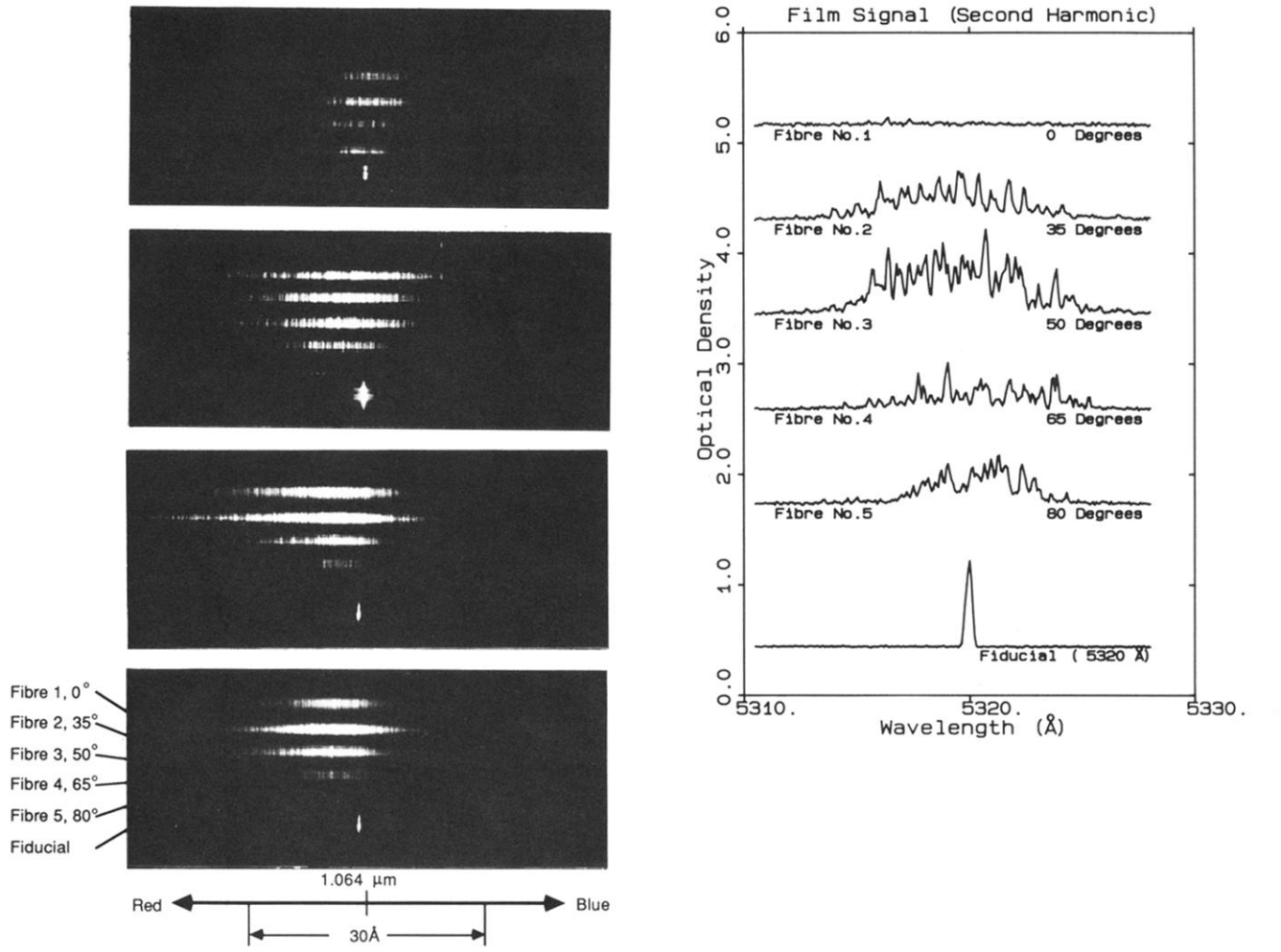

FIG. 2. Set of time-integrated $2\omega_0$ spectra obtained using a laser of wavelength 10 640 Å incident on planar glass targets with pulse lengths (a) 20 psec, (b) 100 psec, (c) 200 psec, and (d) 400 psec. The energy was within the range 1–2 J, the intensity $0.5-1.8\times10^{15}$ W/cm^2, and the experimental setup was that of Fig. 1. The five angles refer to the direction of view of the optical fibers relative to the backscatter direction. A sixth fiber indicates the $2\omega_0$ fiducial (5320 Å). (e) Microdensitometer traces of the 20-psec data in Fig. 2(a).

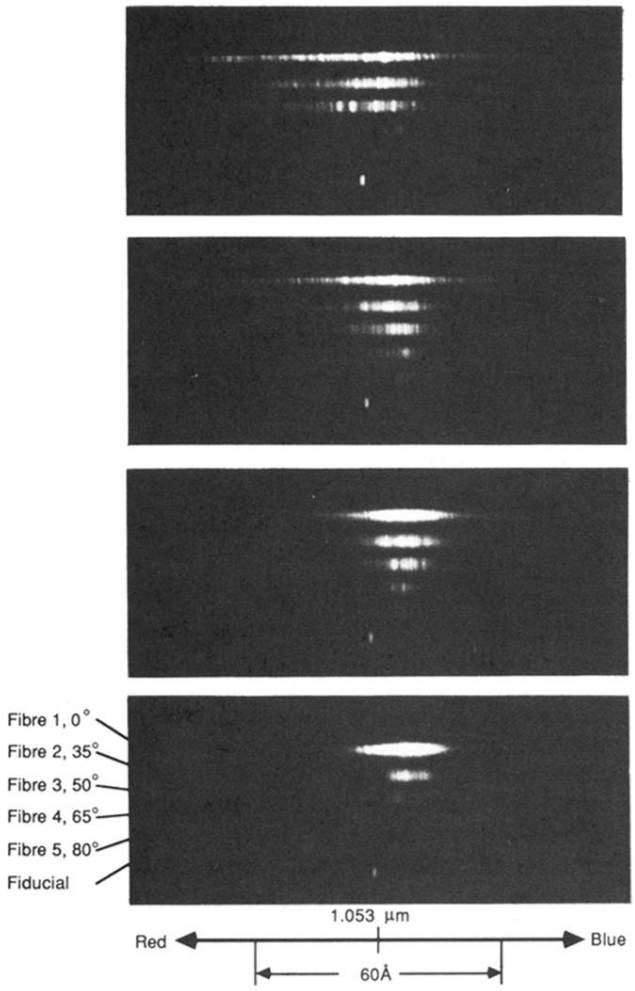

FIG. 4. Time-integrated $1\omega_0$ spectra produced by planar glass targets irradiated with a laser of wavelength 10 530 Å, pulse length 100 psec, energy 2.5 J, and incident intensities of (a) 5×10^{15} W/cm^2, (b) 1×10^{15} W/cm^2, (c) 3×10^{14} W/cm^2, and (d) 3×10^{13} W/cm^2.